

# The influence of domain walls in the incommensurate charge density wave state of Cu intercalated 1T-TiSe<sub>2</sub>

Shichao Yan<sup>1</sup>, Davide Iaia<sup>1</sup>, Emilia Morosan<sup>2</sup>, Eduardo Fradkin<sup>1</sup>, Peter Abbamonte<sup>1</sup> and Vidya Madhavan<sup>1,\*</sup>

<sup>1</sup>*Department of Physics and Frederick Seitz Materials Research Laboratory,  
University of Illinois Urbana-Champaign, Urbana, Illinois 61801, USA and*

<sup>2</sup>*Department of Physics and Astronomy, 6100 Main Street, Rice University, Houston, TX 77005, USA*

We report a low-temperature scanning tunneling microscopy study of the charge density wave (CDW) order in 1T-TiSe<sub>2</sub> and Cu<sub>0.08</sub>TiSe<sub>2</sub>. In 1T-TiSe<sub>2</sub> we observe a long-range coherent commensurate CDW (C-CDW) order. In contrast, Cu<sub>0.08</sub>TiSe<sub>2</sub> displays an incommensurate CDW (I-CDW) phase with localized C-CDW domains separated by domain walls. Density of states measurements indicate that the domain walls host an extra population of fermions near the Fermi level which may play a critical role in the emergence of superconductivity in this system. Fourier transform scanning tunneling spectroscopy studies show that the dominant mechanism for CDW formation in the I-CDW phase is electron-phonon coupling.

Charge density waves (CDW) and superconductivity are two fundamental collective quantum states in solids. The interplay between these states and the nature of co-existing, competing phases in general are long standing questions in solid-state physics [1–4]. 1T-TiSe<sub>2</sub> exhibits both the CDW and superconducting phases which can be tuned by various parameters such as pressure, field, and doping [5–7] making it an ideal system to study this interplay. At 202 K and ambient pressure, 1T-TiSe<sub>2</sub> undergoes a phase transition to a 2×2×2 commensurate CDW (C-CDW) order [8] whose origin has been the subject of a long time debate [9–12]. Superconductivity emerges when the C-CDW phase is suppressed by applying pressure [5], electrostatic gating [6] or through Cu intercalation [7]. Upon Cu intercalation for example, the C-CDW transition temperature quickly drops and the superconducting phase emerges from  $x \sim 0.04$  and reaches the maximal superconducting transition temperature of  $\sim 4.2$  K at  $x \sim 0.08$  [7]. At first glance, this phenomenology suggests that the CDW order and superconductivity are competing phases in this system [7]. Recent studies however indicate that there might be a more exotic and complex interplay between the CDW state and superconductivity: X-ray diffraction and electronic transport experiments report the emergence of an incommensurate CDW (I-CDW) phase which may play an important role in the appearance of superconductivity [6, 14, 15].

Incommensuration may occur through two mechanisms, one through a slight change of the CDW wavevector away from commensuration, and the other through the emergence of phase shifted domains [16–19]. The idea that the incommensurate CDW state in 1T-TiSe<sub>2</sub> occurs through the development of domains was first suggested by Y. I. Joe *et.al*, based on X-ray scattering studies of samples under high pressure. The authors further proposed that superconductivity first nucleates in the domain walls separating the domains [14]. A similar picture was used to explain the Little-Parks effect in the superconducting state of electrostatically gated 1T-TiSe<sub>2</sub> [6]. Very recently, based on the X-ray diffraction measure-

ments, A. Kogar *et.al* reported an I-CDW phase near the superconducting dome in Cu<sub>x</sub>TiSe<sub>2</sub> [15]. These observations taken together strongly suggest that the I-CDW phase may be an important precursor to superconductivity in the 1T-TiSe<sub>2</sub> materials class. It is therefore critical to not only confirm the existence of domain walls in the I-CDW phase of 1T-TiSe<sub>2</sub> but to also measure their effect on the local electronic structure. To do this, we use low-temperature scanning tunneling microscopy (STM) and spectroscopy (STS) to directly probe the real-space characteristics of CDW order in pristine 1T-TiSe<sub>2</sub> and optimally doped Cu<sub>x</sub>TiSe<sub>2</sub> samples (Cu<sub>0.08</sub>TiSe<sub>2</sub>). Note that all the data in this paper was obtained at 6 K in the normal state of the system above the superconducting transition temperature of approximately 4.2 K.

1T-TiSe<sub>2</sub> and Cu<sub>0.08</sub>TiSe<sub>2</sub> samples were cleaved at 77 K and in ultra-high vacuum (UHV), and immediately inserted into STM head. Differential conductance spectra ( $dI/dV$ ) were acquired at 6 K using a standard lock-in technique with 4 mV<sub>rms</sub> modulation at a frequency of 987.5 Hz. 1T-TiSe<sub>2</sub> consists of two-dimensional Se-Ti-Se sandwich layers in which the Se-atom sheets have a hexagonal close-packed structure and the Ti atoms are in the octahedral centers defined by the two Se-atom sheets (Fig.1(a)). TiSe<sub>2</sub> cleaves between the Se-Ti-Se sandwich layers terminating in a Se surface. A schematic of the 2×2 C-CDW order in one of the Se-Ti-Se sandwich layers is shown in Fig.1(b). The 2×2 superstructure and the randomly distributed atomic defects on TiSe<sub>2</sub> surface can be clearly resolved in the STM topography as shown in Fig.1(c) [20]. Correspondingly, the Fourier transform (FT, inset of Fig.1(c)) reveals peaks at half of the Bragg reciprocal-lattice vectors. Typically, in the CDW phase, one observes a gap in the density of states near the Fermi level ( $E_F$ ). Fig.1(d) shows a typical  $dI/dV$  obtained on TiSe<sub>2</sub> away from the native atomic defects. While the density of states is certainly suppressed near  $E_F$ , it remains finite and non-zero, consistent with a partial rather than a full gap. From the change in slope around -110 mV and +10 mV, we deduce a partial gap

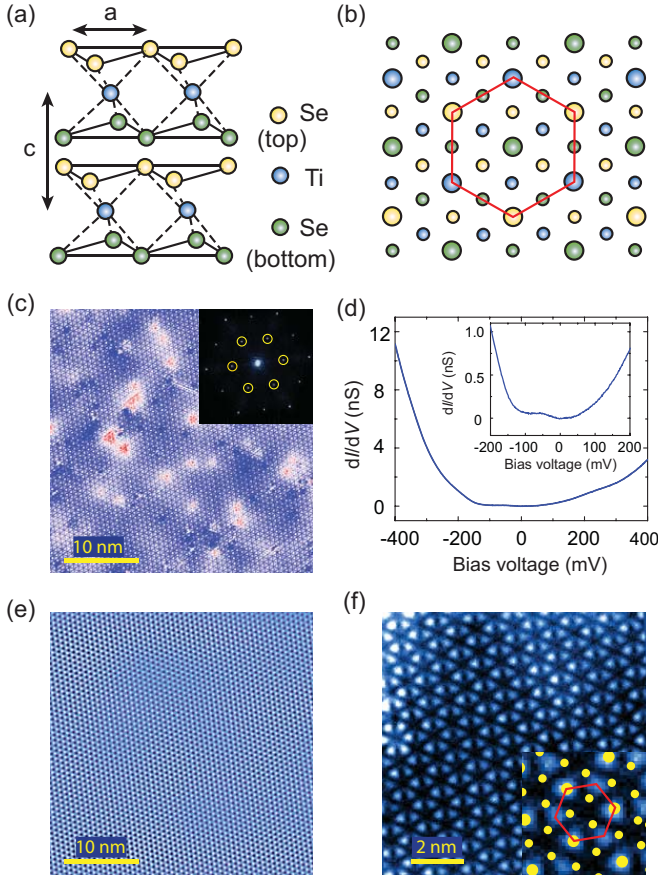


FIG. 1: (a) Schematic crystal structure of the  $1T$ - $\text{TiSe}_2$ . (b) Schematic of the CDW order distribution in the Se-Ti-Se sandwich layer. The larger and smaller circles represent the CDW maxima and minima. The red hexagon highlights the pattern formed by the CDW maxima in the top two (Se- and Ti-) layers. (c) STM constant current topography with  $V_s = -250$  mV,  $I = 100$  pA. The inset shows its Fourier transform. The yellow circles indicate the peaks in the FT due to the CDW order. (d) Typical  $dI/dV$  spectra on  $\text{TiSe}_2$  surface.  $V_s = -400$  mV,  $I = 1$  nA. The inset shows the  $dI/dV$  near the Fermi level. (e) Inverse Fourier transform of only the CDW peaks shown within the yellow circles in (c). (f)  $dI/dV$  map over a  $10 \text{ nm} \times 10 \text{ nm}$  area at  $V_s = 100$  mV. The inset is a zoom-in  $dI/dV$  map. The large and small yellow dots represent the CDW maxima and minima in the top Se layer. The red hexagon highlights the six-lobe hexagonal structure seen in the map. The set up condition is  $V_s = -400$  mV,  $I = 1$  nA.

energy scale of  $\sim 120$  mV which is consistent with angle-resolved photoemission spectroscopy (ARPES) measurements [13, 21, 22].

To expose the charge distribution in the CDW phase and to separate it from the atomic corrugation it is necessary to look at differential conductance maps ( $dI/dV$  map). A  $dI/dV$  map at a fixed bias voltage ( $V_s$ ) represents the spatial distribution of the local density of states at a particular energy ( $eV_s$ ). From the  $dI/dV$  map in Fig.1(f) we find that the charge distribution consists of

hexagonal structures with six lobes. The inset of Fig.1(f) shows the relative positions of the six-lobed hexagon and the CDW pattern on the top Se-layer (yellow dots). Interestingly, while three lobes of the observed hexagonal structure are directly located on the CDW maxima of the top Se-layer, the other three lobes are located between three CDW minima (smaller yellow dots) of the top Se-layer. Comparing this to the schematic CDW pattern in the Se-Ti-Se sandwich layer in Fig.1(b), we conclude that our  $dI/dV$  maps reveal the CDW order in the top Se-layer as well as the Ti-layer underneath. We note that the CDW structure revealed by the  $dI/dV$  maps is not consistent with the simple chiral CDW phase reported in previous STM measurements [23], although more subtle chiral phase cannot be excluded.

STM images allow us to determine the ordering length scale and homogeneity of the CDW order. By carefully studying the CDW pattern shown in Fig.1(e), we conclude that it consists of a single domain whose FT (Fig.1(c) inset) shows sharp peaks at the wave vector corresponding to  $2 \times 2$  C-CDW state. However, a better way to isolate the spatial characteristics of the CDW is to obtain an inverse Fourier transform (I-FT) of only the CDW peaks in the FT. The resulting image (Fig.1(e)) clearly shows a uniform CDW order over the  $40 \text{ nm}$  length scale of the image. In fact, I-FTs of areas as big as  $115 \text{ nm}$  (see Supplemental Materials (SM), [24]) also show an equally uniform CDW pattern with no domain walls indicating that despite the presence of intrinsic atomic scale defects, the CDW phase is long-range ordered in this system.

Next we study the Cu intercalated sample,  $\text{Cu}_{0.08}\text{TiSe}_2$ . The STM images show a large number of atomic scale protrusions on the surface (Fig.2(a)), which can be identified as Cu atoms or clusters on the top layer based on their absence on the pristine  $1T$ - $\text{TiSe}_2$  surface (see SM, [24]). The Cu atoms in the layer beneath can also be imaged at higher bias voltages. The observed density obtained from the layer underneath is consistent with a nominal doping of 8% (see SM, [24]).

We now investigate the fate of the CDW in  $\text{Cu}_{0.08}\text{TiSe}_2$ . Initial transport studies indicate that the C-CDW order parameter is heavily suppressed and is eventually destroyed as superconductivity emerges [7]. However, an I-CDW phase coexisting with superconductivity has been proposed [6, 14, 15]. Turning now to our data (Fig.2(a)), it is immediately clear that a CDW order persists in  $\text{Cu}_{0.08}\text{TiSe}_2$  as can be seen in the clean area between the individual Cu adatoms or clusters. The CDW pattern at first glance looks very similar to  $2 \times 2$  CDW seen in the pristine  $1T$ - $\text{TiSe}_2$  samples. The Fourier transform of the  $\text{Cu}_{0.08}\text{TiSe}_2$  STM topography (inset in Fig.2(a)) is however different from that of the parent compound. Instead of one CDW peak, we now have a pair of CDW peaks in each direction. Naively taking the I-FT of these pairs we find that the resultant CDW

pattern is extremely inhomogeneous (Fig.2(b)). Tracking the CDW pattern across the inhomogeneous regions of the I-FT images suggests that the inhomogeneity may be due to phase shifts in the CDW pattern. This provides the impetus to carefully study high-resolution STM images (Fig.2(c)) where we can now identify many domain walls. The domain walls form long stripes (orange lines in Fig.2(c)) and exist in all three equivalent directions in the sample. Zooming in to a single domain wall (see SM, [24]), we can see the  $\pi$ -phase shift across the domain wall. Overall, this behavior is similar to the I-CDW phase observed in 1T-TaS<sub>2</sub> [16, 17, 19, 25]. Our data indicate that Cu-intercalation has changed the nature of the CDW from a commensurate to an incommensurate phase characterized by domains.

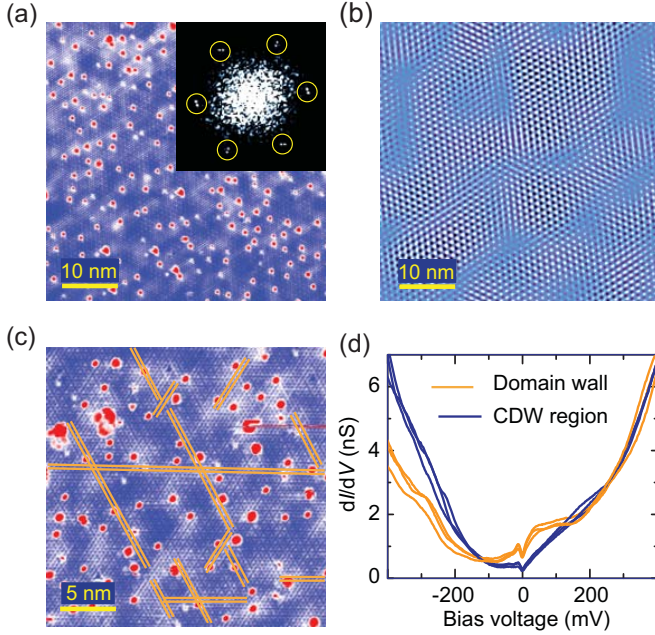


FIG. 2: (a) STM topography with  $V_s = -100$  mV,  $I = 20$  pA. The inset is the Fourier transform of (a) and the yellow circles indicate the position of the CDW peaks. (b) Inverse Fourier transform by filtering the CDW components in the yellow circles of (a) inset. (c) STM topography with  $V_s = -150$  mV,  $I = 20$  pA. The orange solid lines indicate the positions of the CDW domain walls. (d)  $dI/dV$  spectra taken on randomly selected CDW regions and CDW domain wall regions. Set-up condition: 500 mV, 2 nA.

The discussion above suggests that the domain structure in the I-CDW phase is accompanied by a splitting of the CDW peaks in the FTs and that I-FTs of the split peaks can be used to capture domain structure. To clarify this relationship, we performed a control experiment on the Cu<sub>0.08</sub>TiSe<sub>2</sub> surface. By moving the STM tip closer to the surface we find that we are able to remove Cu atoms (see SM, [24]). Furthermore, we find that the domains in the Cu intercalated system can be perturbed by high STM bias voltages. Using these two techniques we

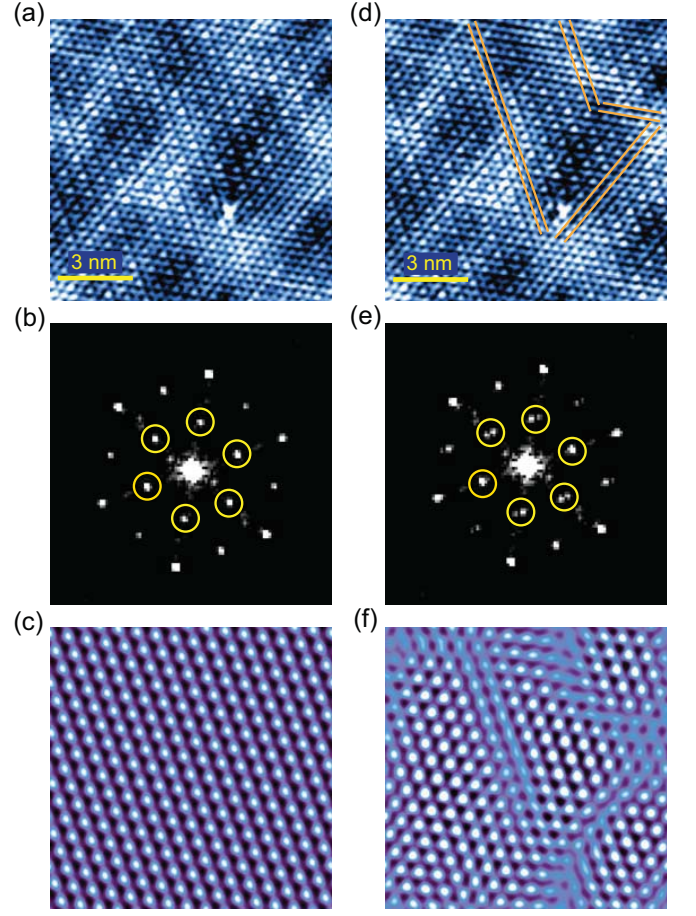


FIG. 3: (a) STM topography obtained on Cu<sub>0.08</sub>TiSe<sub>2</sub> after removing the Cu atoms with STM tip. Set-up condition:  $V_s = -150$  mV,  $I = 20$  pA. (d) STM topography on the same area after CDW domain walls are created (as shown in the orange solid lines). (b) and (e) are the Fourier transforms of (a) and (d), respectively. The yellow circles indicate the position of the CDW peaks in (b). The splitting of the CDW peaks is clearly evident in the yellow circles in (d). (c) and (f) are the inverse Fourier transforms by filtering the CDW components in the yellow circles of (b) and (e), respectively.

now show that the peak splitting is a direct consequence of the presence of domains. Fig.3(a) is an area of the Cu intercalated surface where the Cu atoms have been removed by the tip. This area shows a single C-CDW domain and the FT shown in Fig.3(b) shows a single set of CDW peaks similar to the pristine TiSe<sub>2</sub> samples. Correspondingly, the I-FT image of the CDW peaks shows a homogeneous CDW order (Fig.3(c)). Scanning the same surface at a bias voltage of -350 mV (see SM, [24]) we were able to create domain walls (Fig.3(d)). The FT of this perturbed image (Fig.3(e)) shows that two of the three CDW peaks are now split (the third CDW peak remains un-split since the domain information in this direction is limited, i.e., there is only a very short section of a domain wall in this direction). The newly created CDW domains can also be clearly resolved in the I-FT shown



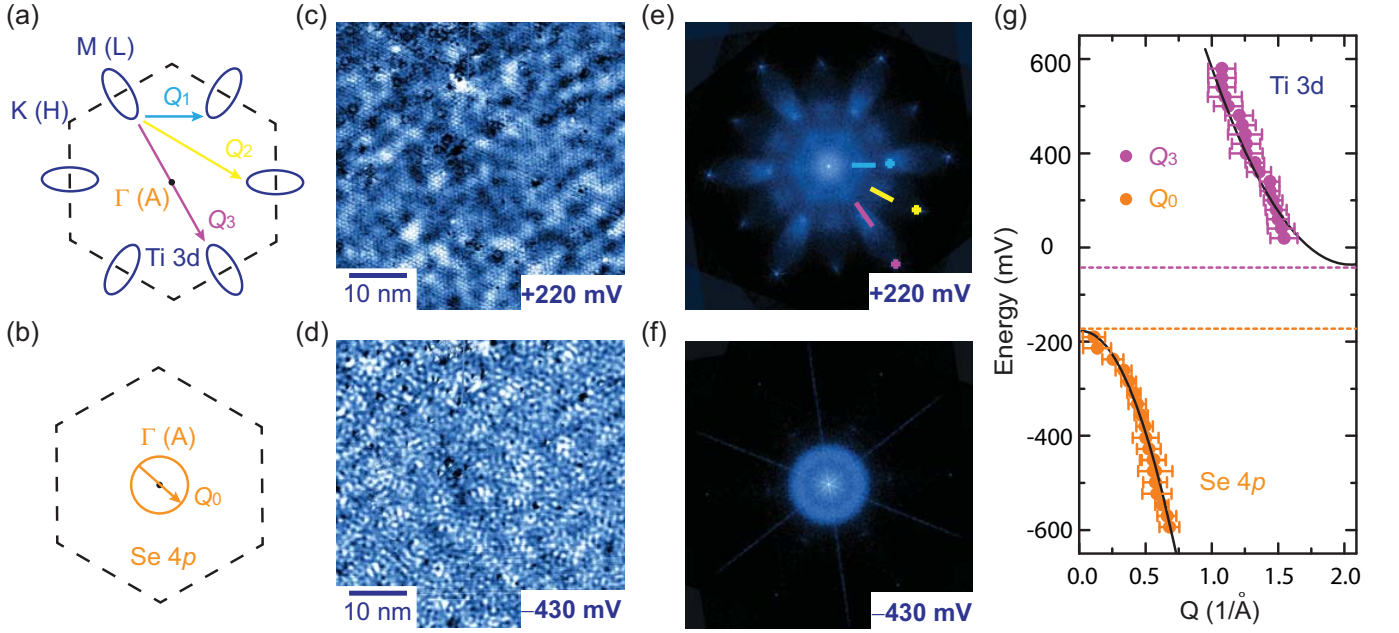


FIG. 4: (a) and (b) The schematics of the Fermi surface topology of Ti-3d derived band (blue ellipses) Se- and 4p derived band (orange circle). The dashed black line is the first BZ.  $\Gamma(A)$ ,  $M(L)$  and  $K(H)$  are the high-symmetry points of the first BZ. The arrows indicate the scattering wavevectors. (c) and (d) Spatially resolved  $dI/dV$  maps at +220 mV and -430 mV. (e) and (f) Drift-corrected and symmetrized Fourier transforms of  $dI/dV$  maps in (c) and (d). (g) Dispersions of  $Q_0$  (orange dots) and  $Q_3$  (pink dots) scattering vectors shown in (a) and (b). The black lines are the parabolic fit to the measured data. The orange and pink dashed lines indicate the top of the Se-4p band and the bottom of the Ti-3d band respectively.

in Fig.3(f). This cements relationship between the split peaks and the domains and also confirms that obtaining I-FT images of the CDW peaks is a good tool to capture the spatial structure of the CDW including the domain walls. Mathematically, the splitting between the peaks reflects the average domain size. From the average ratio between the peak splitting ( $\Delta_{\text{CDW}}$ ) and the C-CDW wavevector ( $Q_{\text{CDW}}$ ) of  $\sim 0.07$  obtained from FTs of large images (see SM, [24]), we obtain a length scale of  $\sim 10$  nm for the average domain size. We note here that the 10 nm size here refers to in-plane I-CDW domains and is consistent with recent X-ray experiments which report  $\sim 13$  nm for the sizes of the I-CDW domains along the  $c$ -axis for  $\text{Cu}_{0.75}\text{TiSe}_2$  samples [15].

Given the proposal that superconductivity might nucleate in the domain walls [6, 14, 15], the natural question is: what is the effect of the domain walls on the local density of states? Unlike impurities that perturb the lattice and electronic structure by adding potentials or strains, the domain walls seen by us represent topological defects in the arrangement of charge. Any effect of such domain walls on the electronic structure is therefore expected to have a non-trivial origin. Fig.2(d) shows  $dI/dV$  spectra obtained on and off domain walls. The spectra on the domain walls show an enhanced density of states near the Fermi level compared to spectra within the localized CDW regions. This intriguing observation indicates that the domain walls host an extra population

of fermions. Furthermore, in the particular case of a period two CDW, the CDW order parameter is expected to go to zero at the domain wall. This combined with the enhanced density of states observed at the domain walls might be important factors leading to the emergence of superconductivity at the domain wall areas.

Having understood the characteristics of the I-CDW phase, we turn our attention to the CDW mechanism in  $\text{Cu}_{0.08}\text{TiSe}_2$ . To explore possible mechanisms, we use Fourier transform of STM  $dI/dV$  maps (FT-STs) to extract the band structure of  $\text{Cu}_{0.08}\text{TiSe}_2$ . (see SM, [24]). FTs of the  $dI/dV$  maps at a given energy contain the allowed scattering vectors ( $Q$ -vectors) between the  $k$ -space electronic states within the constant energy contour (CEC) at that energy. We obtain the energy-dispersion relation by tracking changes of the  $Q$ -vectors with energy. Note that due to the propensity of the surface Cu atoms to move with the tip, it is not possible to obtain noise free  $dI/dV$  maps on surfaces in the presence of Cu atoms.  $dI/dV$  maps were therefore obtained on areas where Cu atoms were deliberately removed by the tip, Fig.4(c) and 4(d). Spectra taken on the cleaned surfaces are almost identical to those on Cu covered surfaces (see SM, [24]). Moreover, even after removing the surface Cu atoms, the CDW remains incommensurate. This indicates that much of the band structure is bulk-like and determined by the doping in the bulk of the sample.

At energies near Fermi level, the band structure of

$\text{Cu}_x\text{TiSe}_2$  is governed by two bands: a Ti-3d band around the L point (at the Brillouin zone (BZ) edge) and an Se-4p band close to the  $\Gamma$  point (the center of the BZ), as shown in Fig.4(a) and 4(b). The Se-4p derived hole-like band has circle-like CECs, and the scattering wavevectors forming a ring in the FT-STs corresponds to the intra pocket scattering ( $Q_0$ , Fig.4(b) and 4(f)). Upon changing  $V_s$  from -600 mV toward  $E_F$ , the ring-like feature in the FT-STs gets continuously smaller and vanishes around -180 mV. No clear dispersive scattering pattern is observed as  $V_s$  ranges between -180 mV and  $E_F$ . For the Ti-3d type band, the CECs consists of six elliptical electron pockets, and there are three main sets of scattering wave vectors ( $Q_1$ ,  $Q_2$ ,  $Q_3$ ) which represent the scattering between the elliptical pockets along  $\Gamma\text{M}$ ,  $\Gamma\text{K}$  and  $\Gamma\text{M}$ , respectively (Fig.4(a) and Fig.4(e)). As the energies increases from  $E_F$  to +400 mV, the sizes of the six elliptical pockets increase and the resulting scattering vectors,  $Q_1$ ,  $Q_2$ ,  $Q_3$  move towards the BZ center (see SM, [24]).

To obtain the dispersion, the position of each scattering wavevector was obtained by a Gaussian fit with a second order polynomial background (see SM, [24]). We focus here on the two strong scattering vectors,  $Q_0$  and  $Q_3$ , and their dispersions are plotted in Fig.4(g). The positions for the top of the Se-4p derived band and the bottom of the Ti-3d derived band are extrapolated by parabolic fit to the extracted data from FT of STM  $dI/dV$  maps. The difference between the valence band top at  $\sim 170$  meV and conduction band bottom band at  $\sim 40$  meV indicates that the band gap is  $\sim 130$  meV which is consistent with the previous ARPES measurements [21, 22]. Our measurements allow us for the first time to directly correlate the I-CDW state with the band structure. Our data indicates that Cu-intercalation moves the Fermi energy into the conduction band. The top of the valance band in these samples is correspondingly further below the Fermi energy compared to pristine  $1\text{T-TiSe}_2$ . There is therefore no nesting of the valance and conduction bands at the wave vector of the CDW. Even assuming that the bands rigidly move to higher energies with rising temperature, by extrapolating from trends from ARPES data [21], we calculate that the valance band will still be far below the Fermi energy at the CDW transition temperature. This rules out Fermi surface nesting as the mechanism for the observed I-CDW. In  $1\text{T-TiSe}_2$ , many studies have suggested that there are both excitonic and phononic contributions to the C-CDW [26–28]. Our data indicate that the excitonic contribution should also be weakened due to the electron doping to the Ti-3d band and the electron-phonon coupling interactions may play a dominant role for the formation of I-CDW in  $\text{Cu}_{0.08}\text{TiSe}_2$  [15].

In conclusion, our data clearly show that the incommensuration due to Cu intercalation proceeds through domain formation. Within each domain, the CDW order is commensurate and the various domains are separated

by sharp domain walls. The emergence of the I-CDW phase as observed by us can be used to explain the loss of long-range coherence of C-CDW phase above the superconducting dome [21, 22] observed in ARPES measurements in the Cu-doped samples. We conclude that the I-CDW phase and associated domain walls should be a common element of  $1\text{T-TiSe}_2$  samples that exhibit superconductivity through doping, gating, or pressure. The enhancement of the density of states in the domain wall may help the emergence of superconductivity. Further STM studies of these samples below the superconducting transition temperature would be important in fully understanding the role of the I-CDW phase in superconductivity.

\* vm1@illinois.edu

- 
- [1] A. H. Castro Neto, Phys. Rev. Lett. **86**, 4382 (2001).
  - [2] S. A. Kivelson, E. Fradkin, and V. J. Emery, Nature **393**, 550 (1998).
  - [3] J. Chang et al., Nat. Phys. **8**, 871 (2012).
  - [4] R. Sooryakumar and M. V. Klein, Phys. Rev. Lett. **45**, 660 (1980).
  - [5] A. F. Kusmartseva, B. Sipos, H. Berger, L. Forr, and E. Tuti, Phys. Rev. Lett. **103**, 236401 (2009).
  - [6] L. J. Li et al., Nature **529**, 185 (2016).
  - [7] E. Morosan et al., Nat. Phys. **2**, 544 (2006).
  - [8] F. J. Di Salvo, D. E. Moncton, and J. V. Waszczak, Phys. Rev. B **14**, 4321 (1976).
  - [9] K. Rossnagel Journal of Physics: Condensed Matter **23**, 213001 (2011).
  - [10] C. Monney, C. Battaglia, H. Cercellier, P. Aebi, and H. Beck, Phys. Rev. Lett. **106**, 106404 (2011).
  - [11] C. Monney et al., Phys. Rev. B **79**, 045116 (2009).
  - [12] H. Cercellier et al., Phys. Rev. Lett. **99**, 146403 (2007).
  - [13] T. E. Kidd, T. Miller, M. Y. Chou, and T.-C. Chiang, Phys. Rev. Lett. **88**, 226402 (2002).
  - [14] Y. I. Joe et al., Nat. Phys. **10**, 421 (2014).
  - [15] A. G. Kogar et al., arXiv: 1608.05957 (2016).
  - [16] B. Burk, R. E. Thomson, A. Zettl, and J. Clarke, Phys. Rev. Lett. **66**, 3040 (1991).
  - [17] B. Burk, R. E. Thomson, J. Clarke, and A. Zettl, Science **257**, 362 (1992).
  - [18] W. L. McMillan, Phys. Rev. B **12**, 1187 (1975).
  - [19] X. L. Wu and C. M. Lieber, Science **243**, 1703 (1989).
  - [20] B. Hildebrand et al., Phys. Rev. Lett. **112**, 197001 (2014).
  - [21] J. F. Zhao et al., Phys. Rev. Lett. **99**, 146401 (2007).
  - [22] D. Qian, et al., Phys. Rev. Lett. **98**, 117007 (2007).
  - [23] J. Ishioka et al., Phys. Rev. Lett. **105**, 176401 (2010).
  - [24] See Supplemental Online Materials for more details.
  - [25] K. Nakanishi, and H. Shiba, J. Phys. Soc. Jpn. **43**, 1839 (1977).
  - [26] J. van Wezel, P. Nahai-Williamson, and S. S. Saxena, Phys. Rev. B **81**, 165109 (2010).
  - [27] J. van Wezel, P. Nahai-Williamson, and S. S. Saxena, Europhys. Lett. **89**, 47004 (2010).
  - [28] M. Porer et al., Nat. Mater. **13**, 857 (2014).